Advances in Engineering Software 190 (2024) 103596

Contents lists available at ScienceDirect

Advances in Engineering Software

journal homepage: www.elsevier.com/locate/advengsoft

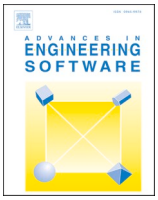

Advanced elasto-plastic topology optimization of steel beams under elevated temperatures

Muayad Habashneh [a], Raffaele Cucuzza [b], Marco Domaneschi [b], Majid Movahedi Rad [a,*]

[a] Department of Structural and Geotechnical Engineering, Széchenyi István University, Győr H-9026, Hungary
[b] Department of Structural, Building and Geotechnical Engineering, Politecnico Di Torino, Corso Duca degli Abruzzi, 24, Torino 10129, Italy

ARTICLE INFO

Keywords:
Topology optimization
Steel beams
Geometrically nonlinear analysis
Elevated temperatures
Thermoelastic-plastic

ABSTRACT

A topology optimization algorithm of steel beams under the influence of elevated temperature, considering the geometrically nonlinear analysis of imperfect structures, is proposed in this work. The proposed methodology is developed for addressing topology optimization problems in the presence of initial geometric imperfections and thermoelastic-plastic analysis by developing the bi-directional evolutionary structural optimization (BESO) method. Two comprehensive examples of lipped channel beams and steel I-section beams are provided to demonstrate the effectiveness of the proposed approach. The considered examples explore the impact of elevated temperature on the topology optimization of imperfect steel beams, considering the interplay between thermal effects, structural imperfections, and nonlinear behavior. The results highlight the significance of integrating temperature effects in achieving optimal and robust steel beam designs. Furthermore, the openings generated by the proposed algorithm can efficiently disrupt the continuous heat flow within the material, leading to regions with reduced thermal conductivity compared to solid regions.

1. Introduction

Structural optimization aims to attain the best structural performance while considering various constraints, such as a specified material volume. There are currently three categories within structural optimization: topology optimization, shape optimization, and size optimization [1–5]. Topology optimization (TO) is a strong and versatile method to find the best material arrangement within a limited design area. It has received much attention in recent decades for solving numerous design challenges in several fields. Therefore, different topology optimization methodologies have been developed for the purpose of finding the optimal material layout of structures [6–12]. In the field of structural topology optimization, two main categories can be distinguished. The first category employs a density-based approach, where each design variable corresponds to a finite element and is used to assess if solid material is present (1) or absent (0). Notably, for this area, the bi-directional evolutionary structural optimization (BESO) approach, among others, has been developed [13]. In the context of the second category, design variables related to structural boundaries are the primary focus, exemplified by techniques like the phase field method [14] and the level set method [15].

The BESO method, at its core, involves simultaneously restoring elements with higher sensitivity numbers while removing elements with the lowest sensitivity numbers [16]. More recently, the BESO method has witnessed significant advancements, enabling its application to a broader range of complex problems beyond traditional structural topology optimization [17–20].

Applications of topology optimization often lead to slender structures that are susceptible to geometric imperfections. The global stability of structures can be significantly affected when structural members experience compression, primarily due to the amplification of initial imperfections caused by nonlinear effects. Hence, ensuring structural stability is of utmost importance during the optimization process [21–24]. By considering uncertain geometrical imperfections, Luo and Zhan [25] proposed an algorithm of topology optimization for solving the worst-case buckling load problems. Furthermore, Movahedi et al. [26] presented a framework for topology optimization that accounts for reliability-based design and considers imperfect analysis. Meng et al. [27] presented a hybrid RBTO method addressing epistemic and aleatory uncertainties. It introduced a triple-nested RBTO model based on fuzzy and probabilistic theory, proposing an efficient single-loop optimization method for deterministic optimization. Tyas et al. [21] introduced an optimization framework that

* Corresponding author.
E-mail address: majidmr@sze.hu (M. Movahedi Rad).

https://doi.org/10.1016/j.advengsoft.2024.103596
Received 12 October 2023; Received in revised form 11 December 2023; Accepted 31 January 2024
Available online 14 February 2024

integrated nominal lateral force load scenarios into a formulation of a plastic linear programming problem in which that approach identified stable solutions for truss optimization. Madah and Amir [28] employed a novel approach to improve truss optimization, addressing stability concerns by integrating structural design and incorporating prescribed initial deviations. Furthermore, by applying the nominal force method for geometric imperfections simulation, Descamps and Filomeno [29] developed a topological optimization algorithm considering stability constraints.

Previous studies in structural optimization have predominantly concentrated on systems subjected to external loads. However, there remains room for improvement, especially in addressing the instabilities arising from thermal problems in structures. Introducing thermal models into the framework of topology optimization presents a valuable opportunity to tackle the complexities associated with design challenges [30–32]. In this context, Rodrigues and Fernandes [33] expanded upon the conventional compliance objective by incorporating both thermal and mechanical loads into their analysis. Li et al. [34] further developed an approach focusing on the optimization of displacement by considering the interaction between thermal and mechanical effects. By considering structures undergoing large deformations, Chung et al. [35] proposed an algorithm that considers nonlinear thermoelasticity. A recent coupled thermo-mechanical RBTO model, promoting computational efficiency, and addressing multi-source uncertainties was proposed by Meng et al. [36]. Gao et al. [37] proposed a topology optimization methodology that accounts for both steady-state temperature and mechanical loads in structures composed of multiple materials. Habashneh and Movahedi [38] proposed a computational technique that applies probabilistic design to thermoelastic topology optimization, incorporating geometric nonlinearity to enhance the optimization process.

Optimizing the geometry of openings or voids within structural components can significantly impact thermal resistance. Several studies have explored determining the optimum geometry of holes or openings in these components to enhance thermal performance. For instance, Yu et al. [39] employed a ray tracing approach to explore how the shapes, alignments, and size distributions of openings impact the thermal conductivity of a structure. Carstensen and Ganobjak [40] introduced a framework aimed at enhancing the optimization of the design of structural elements subjected to mechanical and thermal stresses. In the research conducted by Vantyghem et al. [41], a topology optimization technique was devised for the purpose of designing innovative insulating masonry blocks in which the algorithm aimed to minimize the thermal transmittance of these blocks. These investigations aim to strike a balance between structural strength and thermal efficiency and are crucial for achieving energy-efficient building designs.

In our previous work, presented in a conference paper [42], our research endeavors to optimize the design of structures under high-temperature conditions by employing the bi-directional evolutionary structural optimization (BESO) method within the framework of elasto-plastic limit analysis. This early work laid the foundation for our current research, which expands upon it by addressing the challenges posed by initial geometric imperfections and incorporating a thermoelastic-plastic analysis. Additionally, in this paper, we explore the impact of the resulting optimized topology on temperature distribution within the structures, further advancing our understanding of their thermal performance. Consequently, our proposed work introduces a novel approach, expanding upon the conventional framework of topology optimization. Through the consideration of both thermal effects and geometric imperfections, our approach strives to produce optimized designs that not only fulfill material and thermal performance criteria but also incorporate realistic structural behavior and enhance robustness by utilizing the developed BESO algorithm.

2. Analysis of thermoelastic-plastic structure

This section considers an illustration of thermoelastic-plastic behavior, encompassing the theoretical foundations, mathematical formulations, and key considerations that govern the optimization problem.

2.1. Elasto-plastic limit analysis

The scenario presented in the plastic limit analysis involves the gradual application of a specific load, denoted as $\boldsymbol{F}_i$, to an elastoplastic body. The formula used for this relative or single-parameter loading is as follows:

$$\boldsymbol{F}_i = m_s\, \boldsymbol{F}_0 \tag{1}$$

In the given context, m_s represents a scalar parameter that monotonically increases and is referred to as the load multiplier. Additionally, $\boldsymbol{F}_0$ denotes the initially predefined loads.

2.2. Thermoelastic-plastic analysis

This section outlines the development of a finite element framework for thermoelastic-plastic analysis, with a focus on incremental plasticity. The formulation includes considerations for temperature effects, where the elastic-plastic stiffness matrix $\boldsymbol{K}_e$ and incremental thermomechanical load $\Delta\boldsymbol{F}$ explicitly account for the impact of thermal loading on the material. The incremental formulation in plasticity involves assuming a segmented linear relationship between stress and strain within the material during small load increments. Furthermore, the formulation employed to address nonlinear problems in this study is grounded in the updated Lagrangian formulation, where the reference position is set as the solution obtained in the preceding phase. This approach is also known as the modified updated Lagrangian or the Eulerian method [43]. Standard derivations of these equations can be found in accessible literature [44,45]. However, a brief description of the elastic-plastic stiffness matrix and the incremental thermomechanical load is described here.

The elastic-plastic stiffness matrix, denoted by $\boldsymbol{K}_e$ is calculated by:

$$\boldsymbol{K}_e = \int_v B(\boldsymbol{r})^T \boldsymbol{C}_{ep} B(\boldsymbol{r}) dv \tag{2}$$

where $B(\boldsymbol{r})$ is the temperature field interpolation function of the position vector $\boldsymbol{r}$, $\boldsymbol{C}_{ep}$ denotes the elasto-plasticity matrix, and v represents the volume of deformed element.

The incremental thermomechanical load $\boldsymbol{\Delta F}$ is defined as:

$$\Delta\boldsymbol{F} = \Delta\boldsymbol{F}_T + \Delta\boldsymbol{F}_M \tag{3}$$

where $\boldsymbol{\Delta F_T}$ and $\boldsymbol{\Delta F_M}$ represent the thermal load and the mechanical load, respectively.

3. Developed framework of the thermoelastic-plastic topology optimization problem

This section introduces the development of the thermoelastic-plastic topology optimization framework, encompassing both mechanical and thermal loading effects. It begins with the essential sensitivity analysis techniques. Following this, the formulation of the thermoelastic-plastic topology optimization problem, including considerations for heat conduction and thermal expansion, is examined. It should be mentioned that this section serves as a pivotal segment in our manuscript, unveiling the considered novel advancements of the proposed algorithm.

3.1. Sensitivity analysis

Incorporating heat conduction [46] into the optimization process entails the calculation of sensitivity numbers, with a focus on elements related to temperature-dependent variables. These sensitivity numbers are determined by defining X_e for the $e-th$ element, which varies based

on the presence or absence of the design variable; specifically, X_e can be ($X_e = 1$) when the design variable exists or ($X_e = \xi_{min}$) when it does not. The sensitivity number, represented as α_e^k for the $e-th$ element in the $k-th$ optimization loop, is established based on the incremental thermomechanical load and includes considerations for the impact of thermal effects on the structural response using the following process:

$$\alpha_e^k = \frac{\partial C}{\partial X_e} = \boldsymbol{f}^T \frac{\partial \boldsymbol{u}}{\partial X_e} + \frac{\partial \boldsymbol{f}^T}{\partial X_e}\boldsymbol{u} = \boldsymbol{f}^T \frac{\partial \boldsymbol{u}}{\partial X_e} + \frac{\partial (\boldsymbol{F}_M + \boldsymbol{F}_T)^T}{\partial X_e}\boldsymbol{u} = \boldsymbol{u}^T \boldsymbol{K} \frac{\partial \boldsymbol{u}}{\partial X_e} + \frac{\partial \boldsymbol{F}_T{}^T}{\partial X_e}\boldsymbol{u}. \tag{4}$$

By taking the derivative of the equation $\boldsymbol{Ku} = \boldsymbol{f} = \boldsymbol{F}_M + \boldsymbol{F}_T$, we get:

$$\boldsymbol{K}\frac{\partial \boldsymbol{u}}{\partial X_e} = \frac{\partial \boldsymbol{f}}{\partial X_e} - \frac{\partial \boldsymbol{K}}{\partial X_e}\boldsymbol{u}. \tag{5}$$

By substituting Eq. (5) into Eq. (4), we can update it as follows:

$$\alpha_e^k = \boldsymbol{u}^T \frac{\partial \boldsymbol{f}}{\partial X_e} + \frac{\partial \boldsymbol{f}^T}{\partial X_e}\boldsymbol{u} - \boldsymbol{u}^T \frac{\partial \boldsymbol{K}}{\partial X_e}\boldsymbol{u} \tag{6}$$

Considering that $\boldsymbol{Ku} = \boldsymbol{f} = \boldsymbol{F}_M + \boldsymbol{F}_T$, thus:

$$\boldsymbol{u}^T \frac{\partial \boldsymbol{f}}{\partial X_e} = \frac{\partial \boldsymbol{f}^T}{\partial X_e}\boldsymbol{u}. \tag{7}$$

From Eqs.(6) and (7), we get:

$$\alpha_e^k = \frac{\partial C}{\partial X_e} = 2\boldsymbol{u}^T \frac{\partial \boldsymbol{f}}{\partial X_e} - \boldsymbol{u}^T \frac{\partial \boldsymbol{K}}{\partial X_e}\boldsymbol{u} \tag{8}$$

In order to mitigate the potential problem of mesh dependence and checkerboard patterns, a filtering approach is used [47,48]. This technique is formally stated as:

$$\alpha_e = \frac{\sum_{j=1}^{N_e} w_{ej}\alpha_j}{\sum_{j=1}^{N_e} w_{ej}} \tag{9}$$

The weight, denoted as w_{ej}, is defined as:

$$w_{ej} = \max\{0, r_{min} - d(e,j)\} \tag{10}$$

The Euclidean distance between the centers of the $e-th$ and $j-th$ elements is represented by $d(e, j)$, whereas the filter radius is given as r_{min}.

3.2. The proposed thermoelastic-plastic topology optimization problem

This section centers on the mathematical representation of optimizing the topology of structures within the context of thermoelastic-plastic analysis without delving into a comprehensive discussion of BESO, as it is well-documented in existing literature [13,49]. Diverse techniques have been devised in the domain of structural topology optimization to optimize the material configuration within a specified design domain. This research employs the BESO method as its preferred approach for topology optimization on account of its notable advantages. By implementing the BESO method, one can efficiently determine the most stable structure for a specified quantity of material through the iterative elimination and addition of components in accordance with their sensitivity values [50,16]. Volume constraints notwithstanding, this algorithm has proven to be efficacious in generating optimal designs. By integrating a filter strategy to mitigate the effects of checkerboard patterns and mesh dependence concerns, the BESO method enhances both the convergence speed and accuracy of the optimization procedure. Furthermore, the BESO method offers adaptability when it comes to specifying the objective function and integrating supplementary design limitations. Our objective is to surmount the constraints of conventional optimization methods and generate inventive and effective designs for steel beams through the implementation of the BESO method. The subsequent sections shall provide an elaborate exposition of the BESO algorithm. The mathematical representation for optimizing the topology of structures specifically involves including constraints related to buckling load factors, plastic limit load multiplier, and material volume is formulated as follows:

$$Minimize: \ C = \boldsymbol{u}^T\boldsymbol{Ku} \tag{11.a}$$

$$Subject\ to: \ V^* - \sum_{i=1}^{N} V_i x_i = 0 \tag{11.b}$$

$$\frac{V^*}{V_0} - V_f \le 0 \tag{11.c}$$

$$x_i \in \{0,1\} \tag{11.d}$$

$$\lambda_j \ge \underline{\lambda} > 0 \tag{11.e}$$

$$m_s - m_p \le 0. \tag{11.f}$$

$$\boldsymbol{Ku} = \boldsymbol{f} \tag{11.g}$$

In this context, the objective is to minimize C, which denotes the mean compliance, $\boldsymbol{u}$ indicates displacement vectors, and $\boldsymbol{K}$ is the global stiffness matrix. The volume of an individual element is denoted as V_i, while the entire volume of the structure is represented by V^*. N refers to the total number of elements. In addition, V_0 represents the volume of the design domain, whereas V_f represents the percentage of volume fraction. The binary design variable $\boldsymbol{x_i}$ takes the value of 0 when an element is absent and 1 when it is present. Eq. (11.e) is a representation of the constraint for buckling load factors. In this equation, λ_j represents the jth buckling load factor that corresponds to the specified load instances, while $\underline{\lambda}$ signifies the lower limit of buckling load factors.

It should be mentioned that as m_s increases, the plastic zones of the body continuously expand, reaching a state of unrestricted plastic flow at a well-defined intensity represented by m_p. Defining the plastic limit state [19] it ensures that the work expended by external forces cannot be negative; hence, $m_s - m_p$ must be less than or equal to zero. Eq. (11.f) incorporates the plastic limit load multiplier limitation. Based on the static principle, it is established that any load multiplier m_s, which is statically acceptable, must be less than or equal to the plastic limit load multiplier m_p that corresponds to the whole design domain. The constraint, denoted as ($m_s - m_p \le 0$), represents the plastic limit load multiplier and signifies the point at which the structure achieves complete plastic collapse, hence concluding the optimization process. Furthermore, this constraint is strategically employed to ensure the feasibility and reliability of the optimization process when dealing with plastic deformations. Conversely, in scenarios characterized by elastic solutions, especially at lower load multipliers, the mentioned constraint is omitted. This exclusion is aligned with the inherent characteristics of elastic responses and allows for a tailored approach to accommodate both plastic and elastic behaviors appropriately.

While Eq. (11.g) introduces a new boundary condition related to thermal analysis, where the loading vector $\boldsymbol{f}$ comprises the combined application of both mechanical loading $\boldsymbol{F}_M$ and thermomechanical loading $\boldsymbol{F}_T$, expressed as $\boldsymbol{f} = \boldsymbol{F}_M + \boldsymbol{F}_T$. Therefore, the displacements that are quantified through the objective function inherently consider the impacts of thermal expansion. In summary, Section 3.3 extends the optimization problem to incorporate thermal considerations, presenting a holistic perspective on the structural response. This unique contribution is pivotal for addressing real-world scenarios where the interplay of mechanical and thermal loading influences the topology of structures.

4. Developed algorithm of thermoelastic-plastic topology optimization utilizing BESO

Following a concise mathematical exposition of the topic, the methodology for addressing the thermoelastic-plastic topology optimization problem under the specified constraints using the enhanced BESO method is shown in Fig. 1. The procedural sequence of the proposed

algorithm may be succinctly outlined as follows:

1. Determining the considered design domain of the problem
2. Performing FEA, as detailed in Section 2.2, specifically referring to Eqs.(2 − 3), followed by the computation of sensitivities outlined in Eqs.(4 − 8).
3. Applying filtering schemes, as per Eqs.(9 − 10).
4. Determining the desired magnitude of the volume to be achieved in the subsequent iteration of the procedure.
5. The process of subtracting and adding elements
6. Repeating the processes outlined in stages 2 to 5 iteratively until all specified constraints are met, and the convergence criteria in Eq. (12) are satisfied

$$error = \frac{\left|\sum_{i=1}^{N}(F_{k-i+1} - F_{k-N-i+1})\right|}{\sum_{i=1}^{N}F_{k-i+1}} \leq \tau \tag{12}$$

The objective function is indicated as F. N represents an integer value indicating the quantity of consecutive loops with consistent compliance values. The permissible level of convergence is symbolized by τ, while the current iteration number being executed is designated as k.

The proposed methodology is implemented through a series of MATLAB and Abaqus scripts, facilitating the optimization process for the considered structural analysis. The MATLAB script serves as the main file orchestrating the entire optimization process. It interfaces with Abaqus, defines key parameters, and conducts iterations to achieve convergence. The script initiates the evolutionary process, adjusting design parameters, and interfacing with Abaqus to perform the necessary finite element analyses. The seamless communication between MATLAB and Abaqus is achieved through data transfer. Key parameters, design updates, and analysis results are appropriately transferred between the two environments, ensuring a cohesive and integrated optimization process.

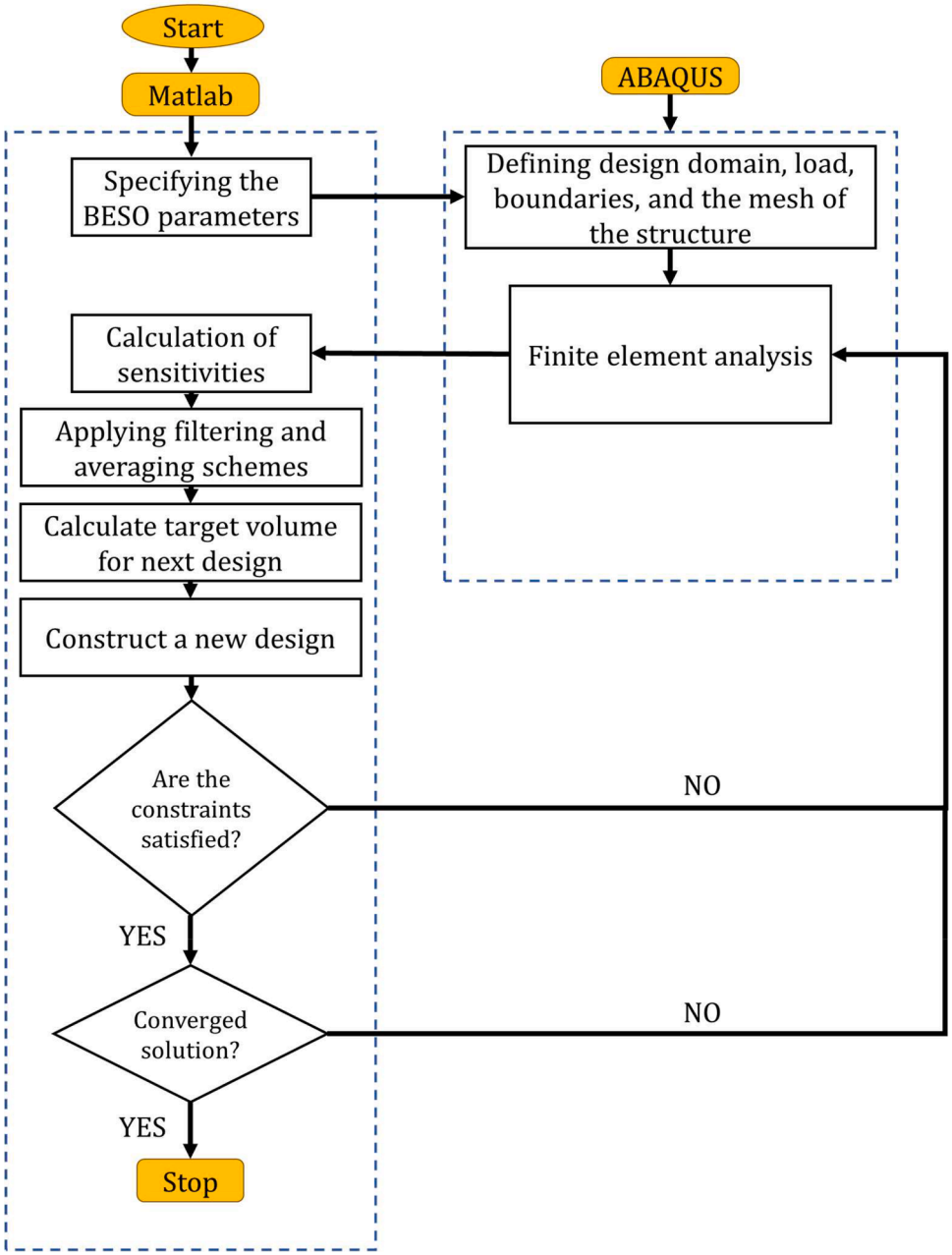

Fig. 1. Flowchart depicting the updated BESO method for thermoelastic-plastic topology optimization.

5. Numerical examples

The topology optimization problem of incorporating thermal analysis of elastoplastic structures while also considering the influence of initial geometric imperfections is addressed by adopting the developed BESO algorithm. The proposed approach's effectiveness and robustness are substantiated through the examination of two numerical models: Firstly, a lipped channel cold-formed steel beam (LCB) is considered the first example, for which the finite element model is validated based on the work of Dolamune and Mahendran [51]. A steel I-section beam is selected as the second example for validation, following the methodology outlined by Prachar et al. [52]. Unless explicitly stated, the BESO parameters utilized in the analysis are as follows: $ER = 1\%$, $AR_{max} = 1\%$, $r_{min} = 96mm$ and $\tau = 0.1\%$. Additionally, the target volume fraction for achieving the desired material distribution is designated as $V_f = 50\%$.

5.1. Lipped channel cold-formed steel beam

The first numerical example in this research focuses on optimizing a Lipped channel cold-formed steel beam. To address the influence of both global and local buckling phenomena, we introduce an initial imperfection using the first two linear buckling modes. To validate the finite element model, we conduct a comparison with prior research conducted by Dolamune and Mahendran [51]. Fig. 2 depicts the beam model, which incorporates symmetrical loading and geometry conditions. Consequently, only half of the span is included in the illustration. Therefore, the considered length of the model is $1250mm$. The model utilized shell elements with a four-node configuration, specifically S4R5 type, with dimensions of $5mm \times 10mm$. The nodes at one end were subjected to tensile and compressive stresses, which resulted in the formation of a triangle force distribution throughout the section and the establishment of a constant bending moment over the whole of the span (Fig. 2.b). The dimensions and the section of the selected LCB are shown in Table 1. Additionally, the beam's supports were modelled using simply-supported boundary conditions for the simulation. The system

Table 1
The dimensions and the section of the selected LCB.

Specification	Magnitude	Cross-section illustration
Grade	250	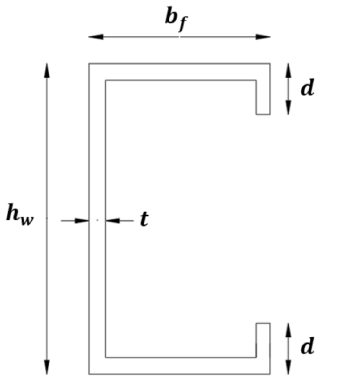
t (mm)	1.95	
h_w (mm)	150	
b_f (mm)	60	
d (mm)	17	
b_f/t (mm)	30.77	
d/t (mm)	76.92	
d/b_f (mm)	2.50	

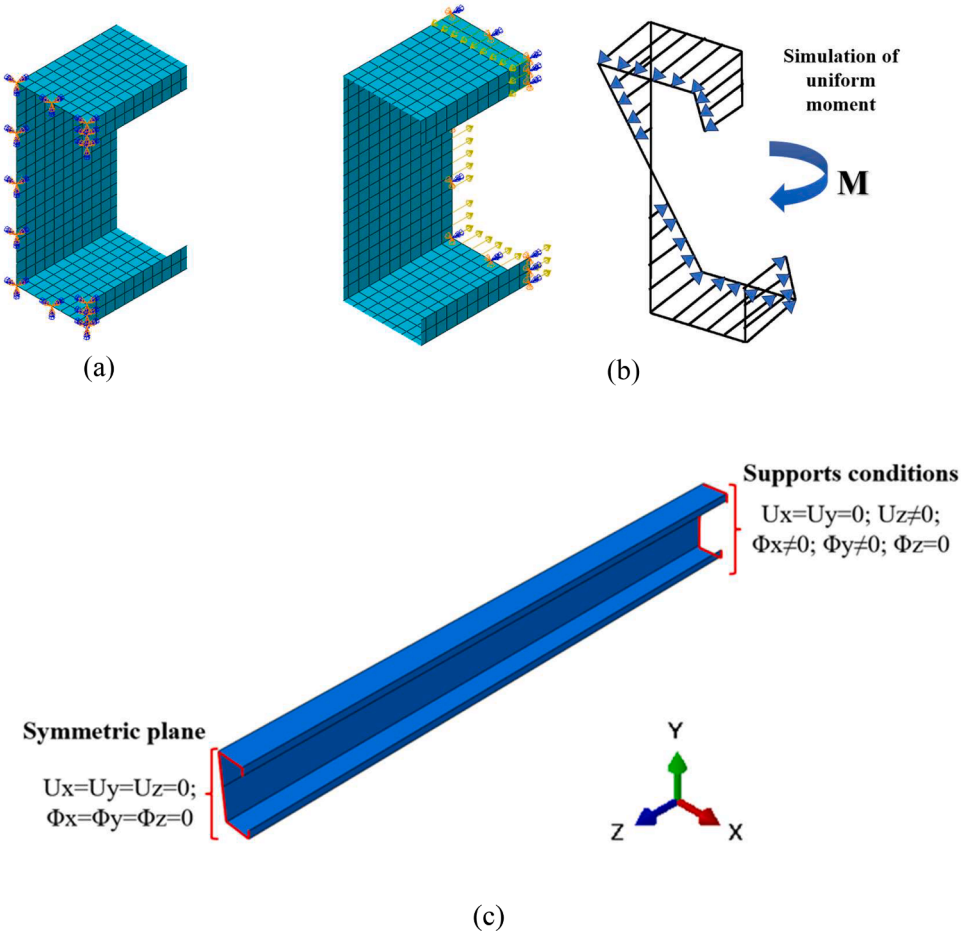

Fig. 2. FEM of LCB: (a) Symmetric plane, (b) Support and applied loads (c) Half span model.

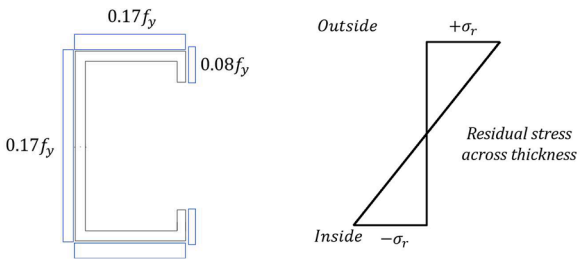

Fig. 3. Residual stress distribution.

Table 2
Mechanical property variation of the chosen steel across different temperatures.

Temperature (°C)	f_y (MPa)	E(GPa)
20	294.0	204.0
300	193.3	145.9
700	36.6	35.7

allows for rotations along both main and minor axes, as well as supporting warping displacement. Simultaneously, it restricts translations and prevents twisting.

Residual stresses existing within cold-formed steel elements exert a notable influence on both the member's stiffness and the potential for premature initial yielding, ultimately resulting in a diminished ultimate strength of the element. Observations commonly indicate that the magnitude of membrane residual stresses in cold-formed steel members tends to be relatively minor when contrasted with flexural residual stresses [53]. Consequently, it is permissible to disregard residual stresses in the membrane. Flexural residual stresses display compressive attributes along the inner surface and tensile attributes along the outer surface of the section. In contrast, the residual stresses within the membrane exhibit either tensile or compressive behaviour and remain consistent throughout its whole thickness. Fig. 3 represents the considered residual stress model of the cold-formed lipped channel.

As the yield strength and elastic modulus of steel decrease at elevated temperatures, the selected steel grade (G250) and thicknesses were adjusted to incorporate the corresponding mechanical property reductions required for high-temperature conditions. Using the reduction factor equations developed by Kankanamge and Mahendran [54], it was possible to determine these reductions in yield strength and elastic modulus. The yield strength and modulus of elasticity values corresponding to each temperature value are presented in Table 2. The analysis made use of stress-strain curves following the model introduced by Ranawaka and Mahendran [55]. For steels exhibiting gradual yielding in their stress-strain curves, a strain-hardening material model was utilized.

During the nonlinear analyses, we considered both residual stresses and the initial geometric imperfections. To incorporate the initial geometric imperfection, the elastic buckling analyses, as shown in Fig. 4, provided the basis for employing the lateral-torsional buckling mode. The choice of buckling modes significantly influences the optimization process, as they define the characteristic deformation patterns at critical loads. In other words, the optimization procedure may struggle to reach an ideal solution if the chosen buckling modes do not precisely reflect the behaviour of the structure. Furthermore, the sensitivity of the objective function and constraints to the design variables is crucial for meaningful design changes during optimization. A geometric imperfection corresponding to $L/1000$ was applied. The equation devised by Lee et al. [56] for calculating flexural residual stresses at ambient temperature was incorporated into the flexural residual stress calculation.

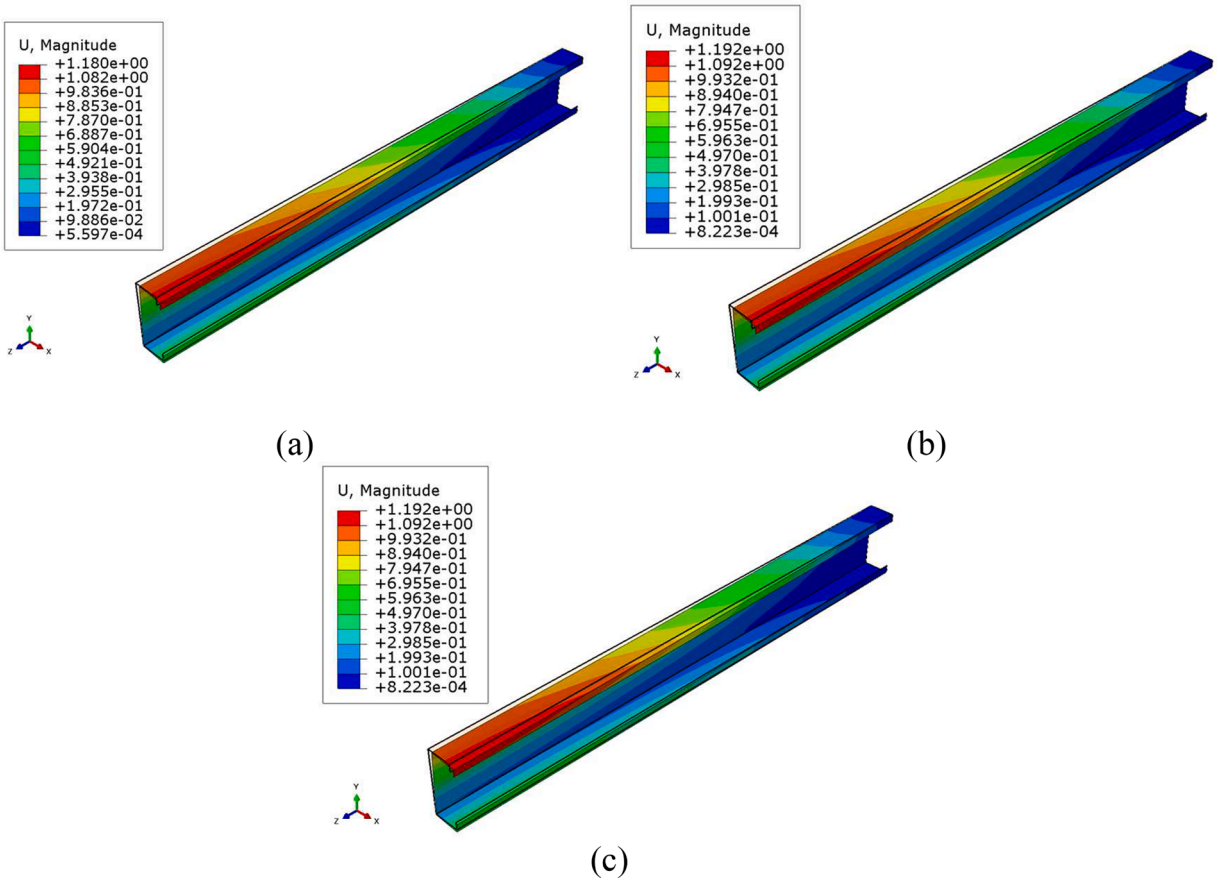

Fig. 4. Modes of elastic lateral–torsional buckling: (a) At 20 °C (b) At 300 °C (c) At 700 °C.

Table 3
Gradual evolution of the material layout until it reaches the optimal solution in the case of 20 °C.

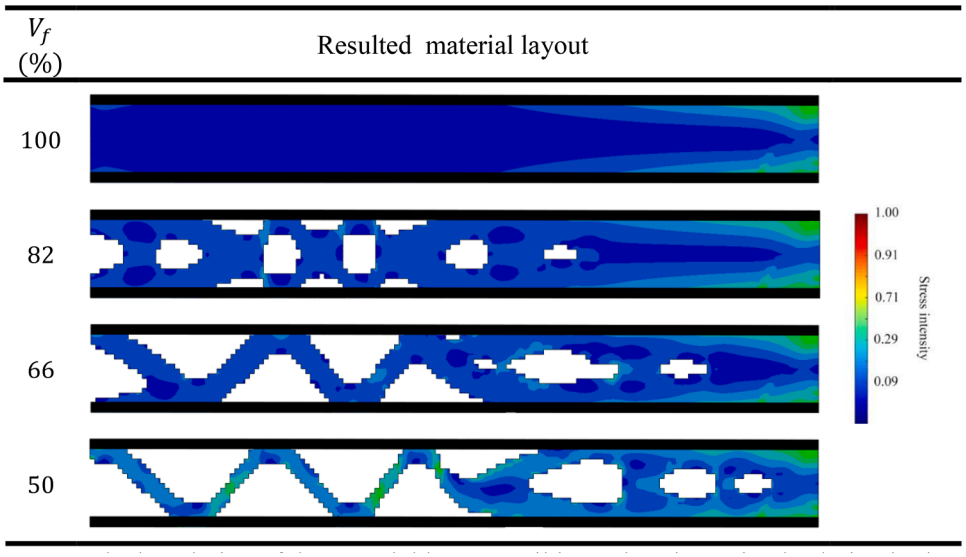

The flexural residual stresses at ambient temperature were assumed to be $0.17f_y$ for the flanges and webs and $0.08f_y$ for the lips [53]. These stresses were assumed to vary linearly across the section's thickness, with compression on the interior surface and tension on the exterior surface.

Three different temperatures are considered in the optimization process which are $20°C$, $300°C$, and $700°C$. Accordingly, Tables 3-5 demonstrate the gradual evolution of the material layout until reaching the optimal solution for different temperature conditions. It should be mentioned that at the beginning of the optimization process, certain parts were excluded and are represented by the color black. In the context of structural topology optimization applied to a half-length representation of a steel lipped section beam, the resultant optimized configuration exhibits a distinctive serpentine morphology at one extremity of the web and perforations at the opposing end, reflecting a dynamic response to the imposed design constraints and loading conditions. It is imperative to underscore that alterations in the temperature conditions yield substantial disparities in the resultant optimized shapes, thereby underscoring the pronounced influence of elevated temperatures on the ultimate optimized configuration of the steel beam.

These findings emphasize the necessity of considering multiple factors, including thermal analysis, elasto-plastic behavior, and initial geometric imperfections, to accurately capture the intricate nature of structural topology optimization under varying temperature conditions.

5.2. Steel I-section beam

This section introduces the second numerical example in this research, which centers on optimizing an I-section beam. To address the influence of global buckling, imperfection is introduced by employing the first two linear buckling modes. It is presumed that the initial geometrical imperfection of the beam is $l/1000$, where l stands for the beam's length. The finite element model is created and verified based on Prachar et al. [52]. Table 6 depicts the cross section, boundary

Table 4
Gradual evolution of the material layout until it reaches the optimal solution in the case of 300 °C.

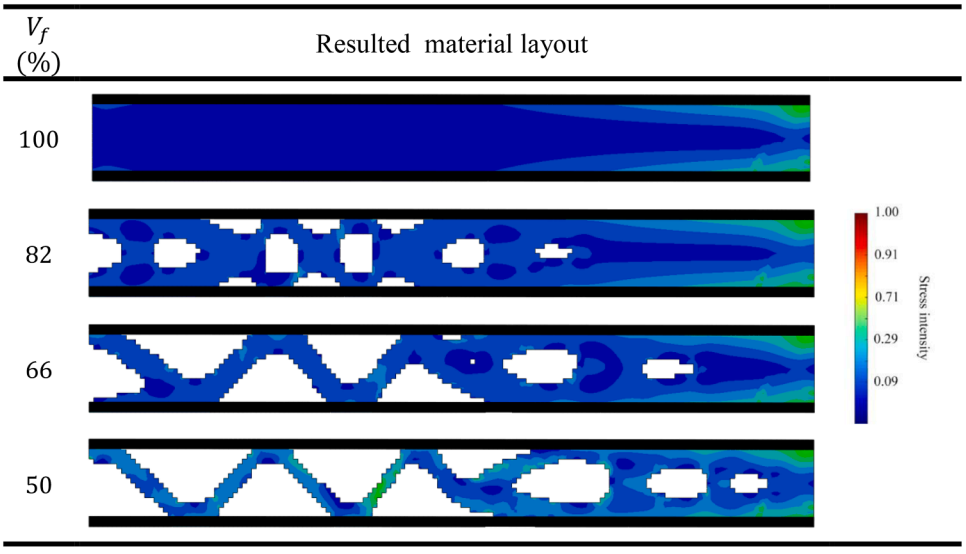

Table 5
Gradual evolution of the material layout until it reaches the optimal solution in the case of 700 °C.

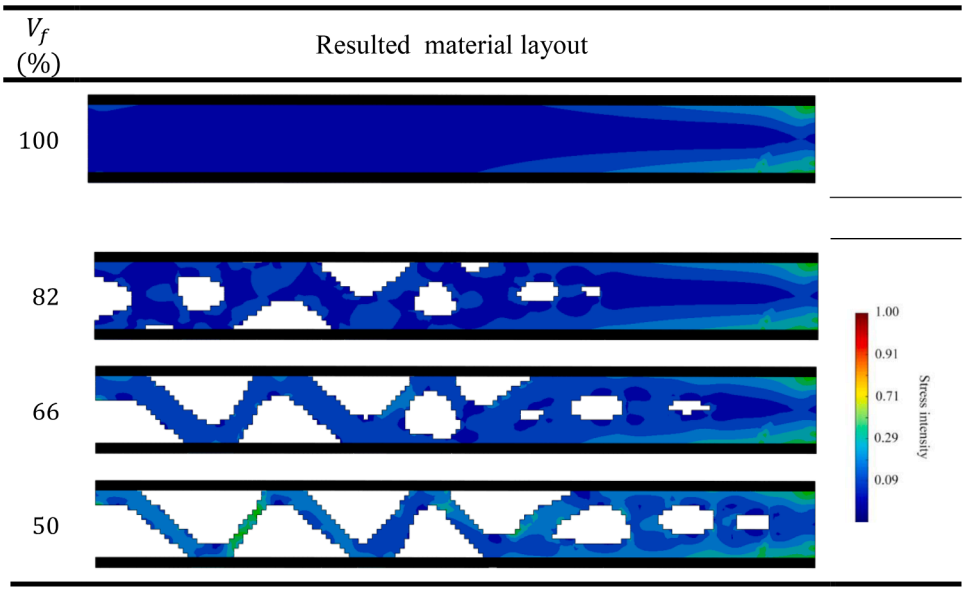

conditions, and geometry of the steel beam.

Fig. 5 illustrates the assembly and the FE mesh of the steel beam in which at one end, the displacements along all axes are restricted. However, at the other end, only along the X and Y axes are constrained. The applied loads are considered at two locations, as it is illustrated in Fig. 5. Furthermore, the beam was simulated using a total of 7456 shell elements (S4-element), each with size of 23*mm*. The shell elements define the geometry of a body at a reference surface. In this particular instance, the thickness is determined by the specification of the section attribute. The element denoted as S4 is a comprehensive and integrated shell element that is designed for general use and capable of accurately modelling finite-membrane-strain behaviour. Each piece is equipped with four integration points.

The residual stress distribution shown in Fig. 6 is taken into consideration in order to allocate the residual stresses to the beam profile. Furthermore, the reduction factors at elevated temperature, namely proportional limit factor ($k_{p,(\theta)}$), yield stress factor $k_{y,(\theta)}$), elastic modulus factor ($k_{E,(\theta)}$) are calculated by $k_{p,(\theta)} = f_{p,(\theta)}/f_{p,(20)}$, and $k_{y,(\theta)} = f_{y,(\theta)}/f_{y,(20)}$, and $k_{E,(\theta)} = E_{(\theta)}/E_{(20)}$, respectively. Fig. 7 depicts how the aforementioned variables change as a function of the temperature. These reduction factors are obtained from established references [57]. The steel grade utilized in this study possesses a yield strength of $355N/mm^2$ and an elastic modulus of $210 \times 10^3 MPa$. The stress-strain data are derived from the formulations outlined in [57]. Fig. 8 exhibits the specific linear buckling modes that have been taken into account. These modes are obtained through a preliminary linear buckling analysis, which enables the identification of the critical buckling behavior of the structure. The resulting mode shapes are subsequently utilized in subsequent steps for the incorporation of imperfections.

The validity of the finite element model is established by a comparison of the load-deflection diagram produced in this research with the results reported by Prachar et al. [52], in which the middle web part of the beam was subjected to elevated temperature. This comparison demonstrates a significant level of agreement, as illustrated in Fig. 9.

This section discusses the results of topological optimization considering the influence of thermoelastic-plastic behavior and initial

Table 6
The geometry, dimensions, cross-section and boundary conditions of the selected beam.

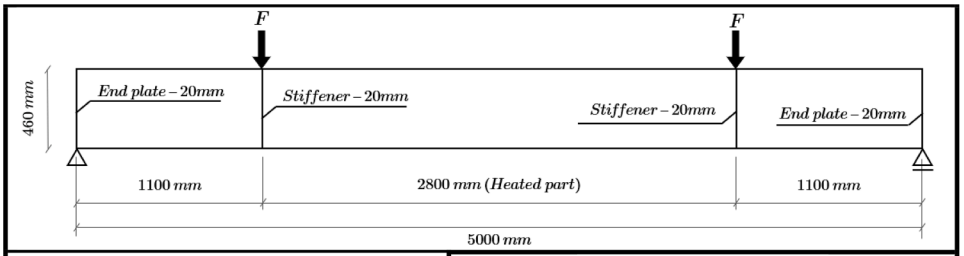

$length\ (mm)$	5000
$h\ (mm)$	460
$B_C\ (mm)$	150
$T_C\ (mm)$	5
$B_T\ (mm)$	150
$T_T\ (mm)$	5
$t\ (mm)$	4

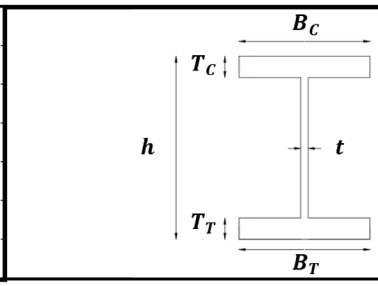

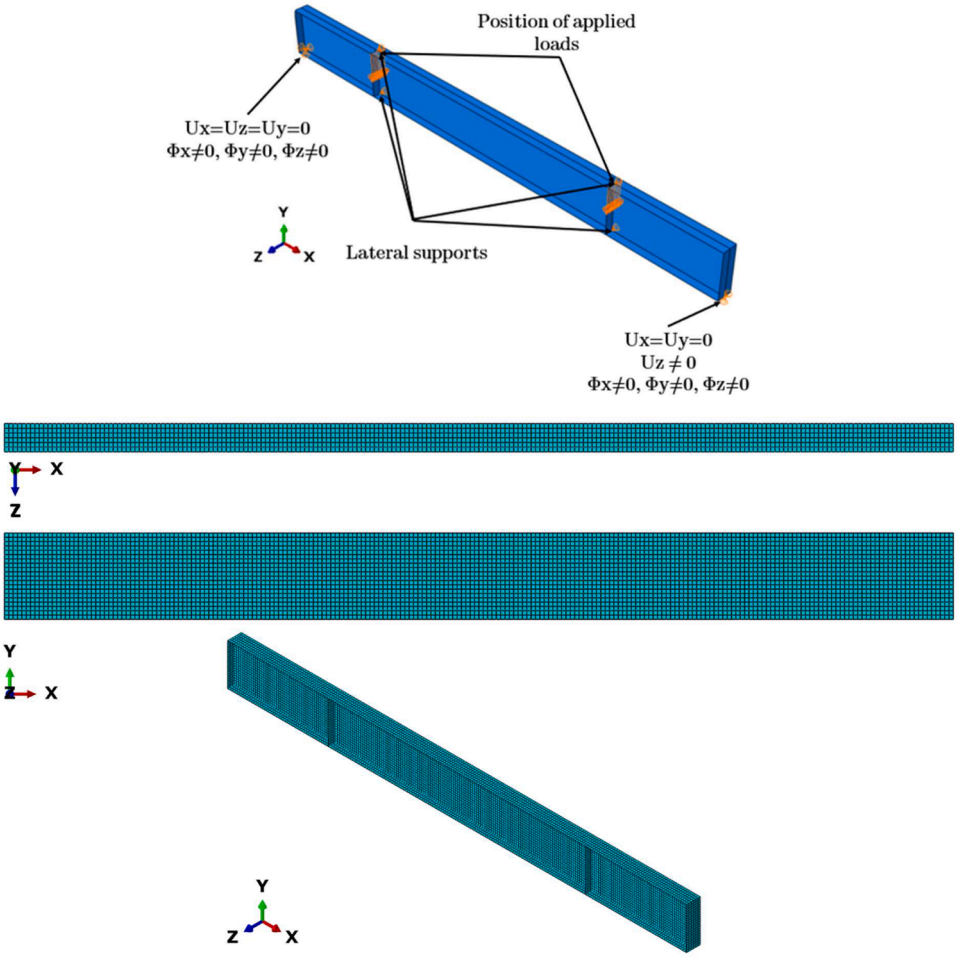

Fig. 5. Assembly and FE mesh of the beam.

geometric imperfections under various temperature conditions, including 20°*C*, 350°*C*, 450°*C*, 550°*C*, 650°*C*, *and*800°*C*. It is essential to note that, in this section, only the middle web portion of the beam is subjected to elevated temperatures. Furthermore, it should be emphasized that the simulation assumes a uniform temperature distribution along the web, maintaining a constant temperature value.

Our analysis involves a comprehensive comparison between the complete structural domain of the beam and the resulting optimized configurations. Our primary focus is the evaluation of ultimate load values under varying temperature conditions, as graphically depicted in Fig. 10. Notably, as the temperature increases, a pronounced trend becomes evident, which is that the disparity in ultimate load capacity between the full structural domain and the optimized configuration steadily diminishes. This observation signifies a critical aspect of structural response under thermal influences.

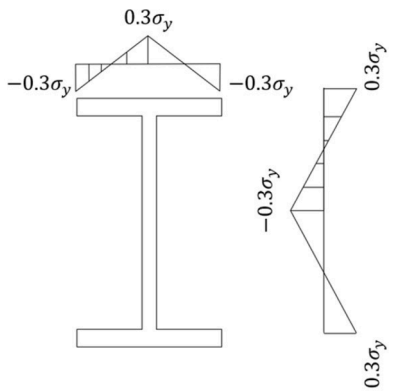

Fig. 6. Residual stress distribution.

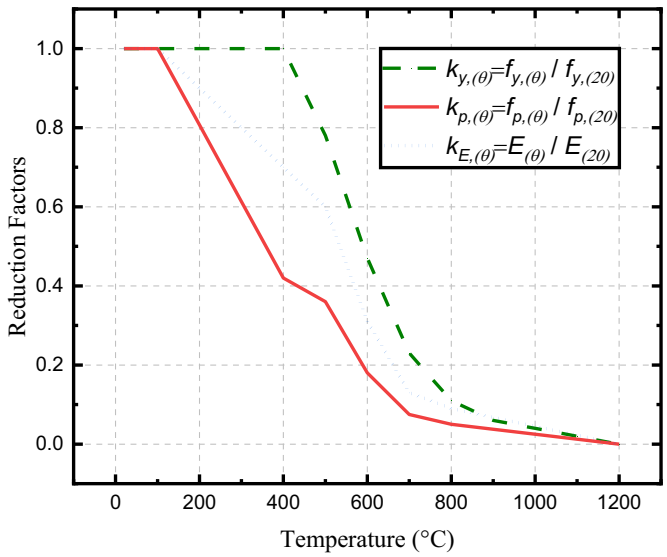

Fig. 7. Considered reduction factors of material properties.

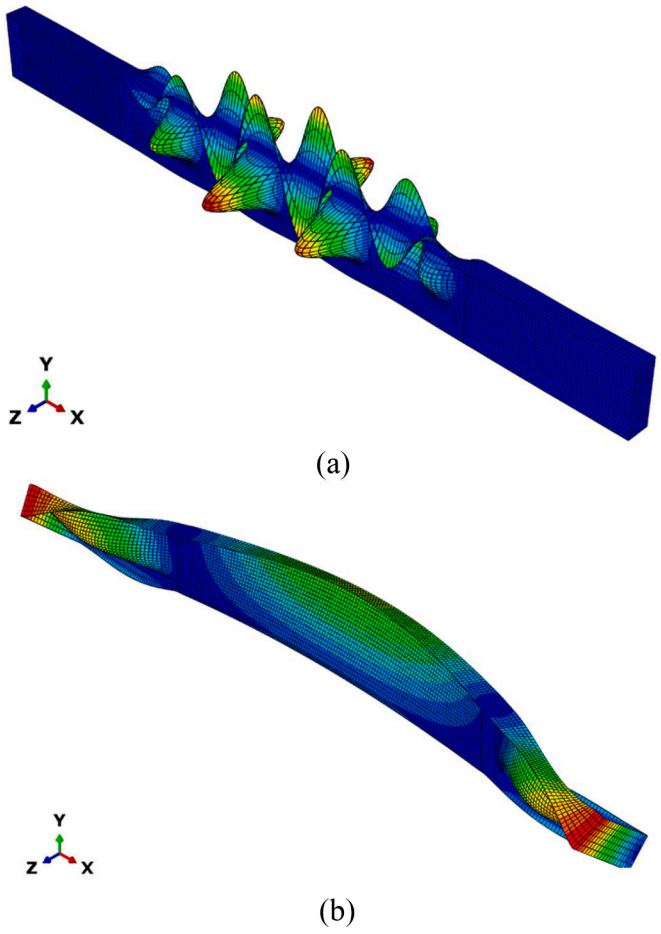

Fig. 8. The considered buckling modes in the model (a) local (b) global.

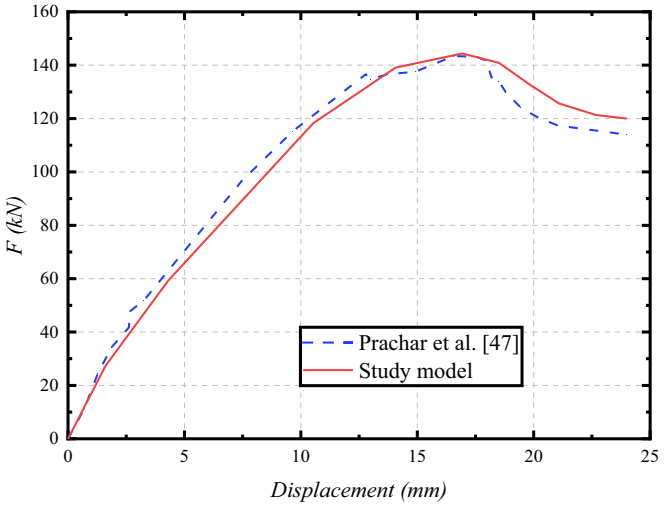

Fig. 9. The obtained numerical results in comparison with the results of Prachar et al. [52].

Table 7 represents the optimized material arrangement, which is close to failure when subjected to plastic limit analysis. The resulting optimal topological shapes exhibit nearly identical material layouts across different temperature scenarios. This is due to considering a uniform temperature distribution with a constant temperature value across the middle part of the web. Only one temperature case is considered here for illustration, specifically the case at 800°C. It's worth

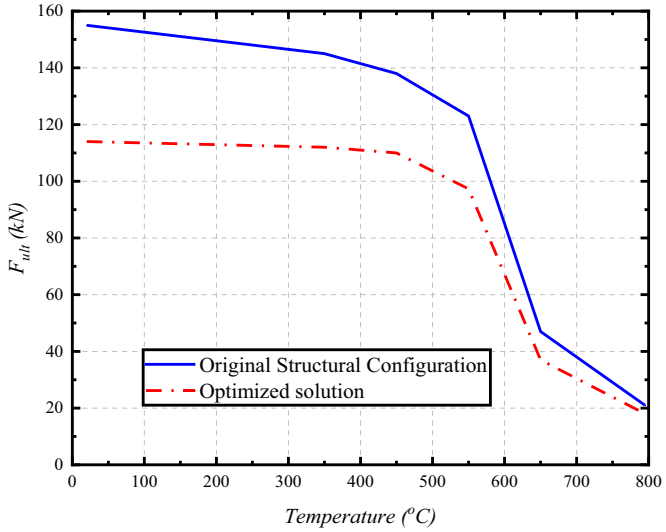

Fig. 10. Obtained ultimate loads for different temperatures in the cases of full domains and optimized solutions.

noting that certain components were initially excluded from the optimization process, visually represented by the use of the color black. Consequently, during the optimization procedure, these excluded sections remained unchanged.

This outcome has significant implications for structural engineering, as it underscores the crucial role of thermal effects in shaping structural behavior. Furthermore, if structures can be designed to perform well under elevated temperatures without overdesigning, it can lead to resource savings, such as reduced material and construction costs. Accordingly, engineers and designers can use this knowledge to develop more robust and efficient structural solutions, optimizing materials and designs to enhance the safety and reliability of structures.

To demonstrate the results of applying the elasto-plastic limit concept, two different temperatures are under consideration: 350°C and 650°C. At a temperature of 350°C, the plastic-limit load multiplier (m_p)is 5.2, the predefined load is denoted as F_0 and equals 21.5kN, while the ultimate load is represented as F_{ult} and is equal to 114kN. For clarity, we examine three load cases: $F_1 = 0.5 \times F_0$, $F_2 = 3.0 \times F_0$, and $F_3 = 5.0 \times F_0$. Conversely, at a temperature of 650°C, the plastic-limit load multiplier (m_p)is 4.5, the predefined load F_0 is 11kN, and the ultimate load (F_{ult}) is 37kN. In this scenario, the three considered load cases are $F_1 = 0.1 \times F_0$, $F_2 = 2.0 \times F_0$, and $F_3 = 3.0 \times F_0$. The resulting optimized shapes of considering the elasto-plastic limit concept for the cases of 350°C and 650°C are presented in Table 8 and Table 9, respectively.

It is noteworthy that in the first scenario, which corresponds to minimal loading, the entire model exhibits elastic behavior. In the second scenario, the presence of plastic zones is nearly imperceptible. Conversely, in the third scenario, significant plastic zones become evident.

Expanding upon our previous analysis of the persistent thermal effects on the web, we redirect our focus toward an additional investigative endeavor. In this phase, we investigate the implications of exposing the lower flange of the steel beam to elevated temperatures distributed uniformly across the entire beam section. This comprehensive exploration encompasses a meticulous examination of topologically optimized configurations across a range of elevated temperature scenarios. Furthermore, it entails a comprehensive evaluation of the associated load characteristics and an assessment of the ultimate load values under varying temperature conditions.

Fig. 11 provides a graphical representation of the evaluation of ultimate load values as temperature varies. This visualization illustrates the progressive impact of temperature on the load-bearing capacity of the beam when the bottom flange is subjected to fire in the cases of the

Table 7
The resulting optimized shape according to the developed algorithm.

Temperature (°C)	Optimized results
800	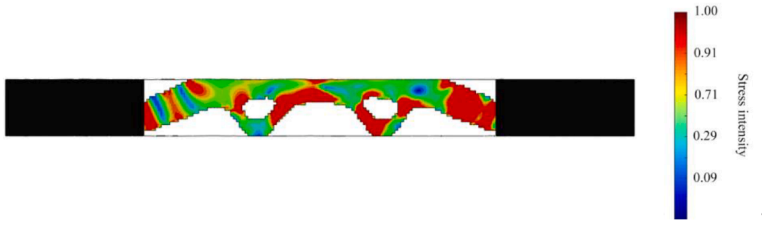

Table 8
The resulted topologies in the case of 350°C according to the elasto-plastic limit concept.

Load case	Optimized results
$F_1 = 0.5 \times F_0$	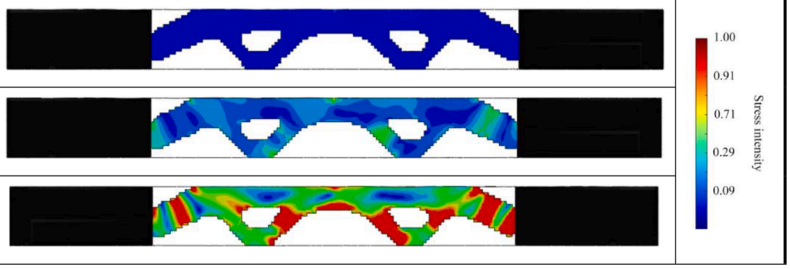
$F_2 = 3.0 \times F_0$	
$F_3 = 5.0 \times F_0$	

full domain and the optimized design. Significantly, it can be seen that when the temperature rises, there is a clear and consistent reduction in the difference in ultimate load capacity between the whole structural domain and the optimized layouts.

Table 10 illustrates the topological optimized shape considering the case, which is the nearest design to the failure by adopting plastic-limit load analysis. During the initial phases of the optimization process, certain components were omitted, as indicated visually by the use of the color black. It is important to note that these excluded sections remained unaltered throughout the optimization process. It should be emphasized that the optimized shapes resulting from the application of the thermoelastic-plastic topology optimization method when the temperature has a varied distribution exhibit nearly the same material distribution of the resulted in optimum designs. As an illustration, the considered case to show the optimized shape in Table 10 is when the applied temperature is 800°C.

To gain a deeper understanding of the effects of elevated temperatures, we present an analysis of the temperature distribution within the beam. This analysis includes a comparative study between the original beam shape and the optimized configuration achieved through the integration of the proposed thermoelastic-plastic topological optimization algorithm. Table 11 serves as a visual aid, offering temperature distribution contours when exposing the lower part of the flange to fire, specifically at temperature levels of 650 °C and 800 °C. Furthermore, this presentation provides insights into the resulting temperature distribution of the optimized beam, emphasizing the influence of topology optimization on temperature profiles.

The results suggest that optimizing the web part of a steel I-beam, leading to the presence of openings has a significant impact on the reduction of the heat distribution within the material. These openings disrupt the continuous flow of heat, resulting in regions with openings exhibiting reduced thermal conductivity compared to solid regions. This

Table 9
The resulting topologies in the case of 650°C according to the elasto-plastic limit concept.

Load case	Optimized results
$F_1 = 0.1 \times F_0$	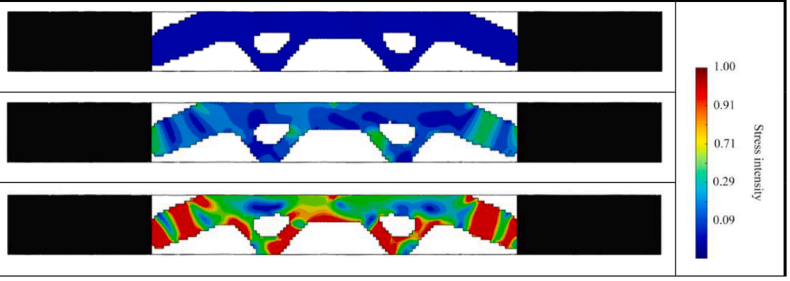
$F_2 = 2.0 \times F_0$	
$F_3 = 3.0 \times F_0$	

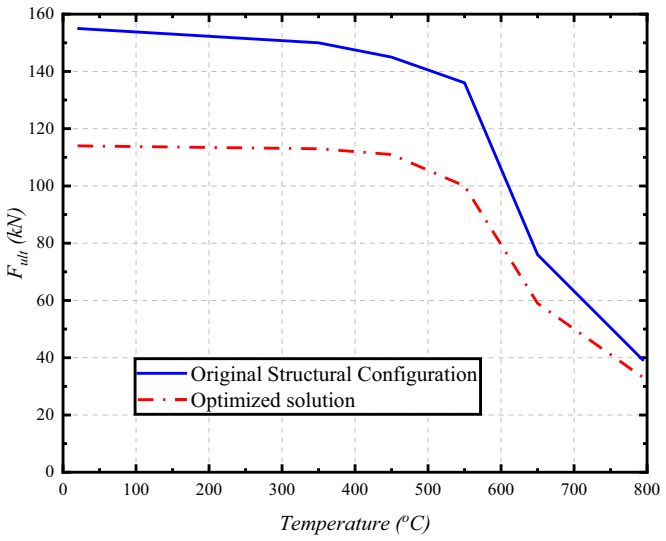

Fig. 11. Obtained ultimate loads for different temperatures in the cases of full domains and optimized solutions with bottom flange exposure to fire.

phenomenon signifies that heat may not efficiently conduct through areas with openings, which can be advantageous in applications where controlled heat dissipation or thermal insulation is desired.

6. Conclusions

This study builds upon the foundation laid in our earlier work [42], introducing the BESO-based approach to optimize the design of structures under high-temperature conditions. However, this journal paper significantly extends the research by addressing the complexities introduced by initial geometric imperfections and incorporating thermoelastic-plastic analysis, providing a more comprehensive and robust approach to structural design under varying temperature conditions. The inclusion of thermal effects and the impact of geometric imperfections on structural topology optimization are novel contributions of this work. In summary, the key points of this study can be highlighted as follows:

- Our findings underscore the necessity of considering multiple factors, including thermal analysis, elasto-plastic behavior, and initial geometric imperfections, to accurately capture the intricate nature of

Table 10
Resulting topologies using the developed algorithm with bottom flange exposure to fire.

Temperature (°C)	Optimized results
800	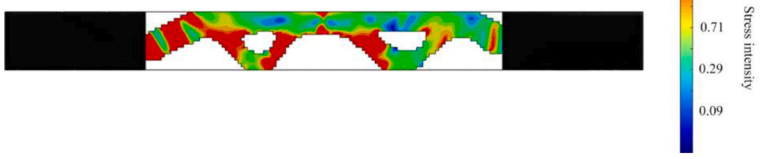

Table 11
Temperature distribution comparison for different design domains under fire exposure.

Temperature (°C)	Design domain	Temperature distribution when applying fire from the bottom flange
650	Original shape	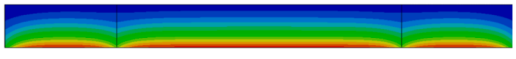 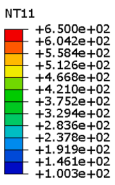
	Optimized shape	
800	Original shape	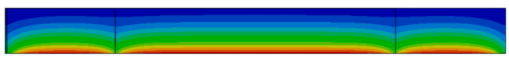
	Optimized shape	 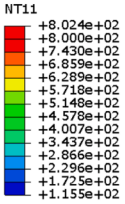

structural topology optimization under varying temperature conditions.

- The examination of temperature distribution inside a steel I-beam reveals that the optimization of the web section, resulting in the incorporation of apertures, has a substantial influence on the dispersion of heat.
- The proposed analysis has shown a trend that indicates that as temperatures increase, the disparity in ultimate load capacity between the full structural domain and the optimized configuration steadily diminishes. This observation highlights the crucial role of thermal effects in shaping structural behavior and has significant implications for structural engineering.
- The optimized shapes adhere to the elasto-plastic limit concept, exhibiting no visible plastic zones under minimal load conditions and progressively displaying a greater presence as the load increases until reaching the greatest load multiplier.
- Our work demonstrates that the strategic optimization of the web section in steel I-beams, which introduces openings, offers a promising avenue for mitigating heat distribution within the material. The presence of these openings disrupts the continuous flow of heat, resulting in regions exhibiting reduced thermal conductivity compared to solid counterparts.

The results shed light on the substantial potential of employing topology optimization in the field of structural engineering to actively manage heat distribution within structural elements. This work opens up exciting avenues for structural engineers, offering them the tools to design structures that not only withstand but thrive under extreme temperature conditions. By optimizing material use and strategically incorporating openings in structural elements, engineers can create more resilient, energy-efficient, and cost-effective structures.

CRediT authorship contribution statement

Muayad Habashneh: Writing – original draft, Conceptualization, Methodology. **Raffaele Cucuzza:** Formal analysis, Conceptualization, Methodology. **Marco Domaneschi:** Visualization, Investigation. **Majid Movahedi Rad:** Supervision, Software, Validation, Writing – review & editing.

Declaration of competing interest

The authors declare that they have no known competing financial interests or personal relationships that could have appeared to influence the work reported in this paper.

Data availability

No data was used for the research described in the article.

References

[1] Cucuzza R, Rosso MM, Aloisio A, Melchiorre J, Lo Giudice M, Marano GC. Size and shape optimization of a guyed mast structure under wind, ice and seismic loading. Appl Sci 2022;12:4875. https://doi.org/10.3390/APP12104875/S1 (Switzerland).

[2] Christensen PW, Klarbring A. An introduction to structural optimization. Solid Mech Appl 2008;153:1–220. https://doi.org/10.1007/978-1-4020-8666-3_1.

[3] Ramm E., Maute K., Schwarz S. Adaptive topology and shape optimization. Computational mechanics, new trends and applications, Barcelona, Spain 1998.

[4] Eschenauer HA, Kobelev VV, Schumacher A. Bubble method for topology and shape optimization of structures. Struct Optim 1994;8:42–51. https://doi.org/10.1007/BF01742933.

[5] Rosso MM, Cucuzza R, Aloisio A, Marano GC. Enhanced multi-strategy particle swarm optimization for constrained problems with an evolutionary-strategies-based unfeasible local search operator. Appl Sci 2022;12. https://doi.org/10.3390/app12052285.

[6] Le C, Norato J, Bruns T, Ha C, Tortorelli D. Stress-based topology optimization for continua. Struct Multidiscip Optim 2010;41:605–20. https://doi.org/10.1007/S00158-009-0440-Y/METRICS.

[7] Nonlinear eigenvalue topology optimization for structures with frequency-dependent material properties, ScienceDirect n.d. https://www.sciencedirect.com/science/article/pii/S0888327022000322 (accessed June 14, 2023).

[8] Kharmanda G, Olhoff N, Mohamed A, Lemaire M. Reliability-based topology optimization. Struct Multidiscip Optim 2004;26:295–307. https://doi.org/10.1007/S00158-003-0322-7/METRICS.

[9] Xu D, Chen J, Tang Y, Cao J. Topology optimization of die weight reduction for high-strength sheet metal stamping. Int J Mech Sci 2012;59:73–82. https://doi.org/10.1016/J.IJMECSCI.2012.03.006.

[10] Wang MY, Wang X, Guo D. A level set method for structural topology optimization. Comput Methods Appl Mech Eng 2003;192:227–46. https://doi.org/10.1016/S0045-7825(02)00559-5.

[11] Blachowski B, Tauzowski P, Lógó J. Yield limited optimal topology design of elastoplastic structures. Struct Multidiscip Optim 2020;61:1953–76. https://doi.org/10.1007/S00158-019-02447-9/FIGURES/20.

[12] Rosso MM, Cucuzza R, Di Trapani F, Marano GC. Nonpenalty machine learning constraint handling using PSO-SVM for structural optimization. Adv Civ Eng 2021;2021. https://doi.org/10.1155/2021/6617750.

[13] Xie YM, Steven GP. A simple evolutionary procedure for structural optimization. Comput Struct 1993;49:885–96. https://doi.org/10.1016/0045-7949(93)90035-C.

[14] Wang MY, Zhou S. Phase field: a variational method for structural topology optimization. CMES-Comput Model Eng Sci 2004;6:547.

[15] Sethian JA. Level set methods and fast marching methods: evolving interfaces in computational geometry, fluid mechanics, computer vision, and materials science, 3. Cambridge University Press; 1999.

[16] Yang XY, Xie YM, Steven GP, Querin OM. Bidirectional evolutionary method for stiffness optimization. AIAA J 1999;37:1483–8. https://doi.org/10.2514/2.626.

[17] Bruns TE, Tortorelli DA. An element removal and reintroduction strategy for the topology optimization of structures and compliant mechanisms. Int J Numer Methods Eng 2003;57:1413–30. https://doi.org/10.1002/nme.783.

[18] Habashneh M, Movahedi Rad M. Reliability based geometrically nonlinear bi-directional evolutionary structural optimization of elasto-plastic material. Sci Rep 2022;12:1–22. https://doi.org/10.1038/s41598-022-09612-z. 2022 12:1.

[19] Movahedi Rad M, Habashneh M, Lógó J. Elasto-plastic limit analysis of reliability based geometrically nonlinear bi-directional evolutionary topology optimization. Structures 2021;34:1720–33. https://doi.org/10.1016/J.ISTRUC.2021.08.105.

[20] Radman A. Combination of BESO and harmony search for topology optimization of microstructures for materials. Appl Math Model 2021;90:650–61. https://doi.org/10.1016/J.APM.2020.09.024.

[21] Tyas A, Gilbert M, Pritchard T. Practical plastic layout optimization of trusses incorporating stability considerations. Comput Struct 2006;84:115–26. https://doi.org/10.1016/J.COMPSTRUC.2005.09.032.

[22] Dalklint A, Wallin M, Tortorelli DA. Structural stability and artificial buckling modes in topology optimization. Struct Multidiscip Optim 2021;64:1751–63. https://doi.org/10.1007/S00158-021-03012-Z/FIGURES/10.

[23] Rozvany GIN. Difficulties in truss topology optimization with stress, local buckling and system stability constraints. Struct Optim 1996;11:213–7. https://doi.org/10.1007/BF01197036/METRICS.

[24] Jalalpour M, Igusa T, Guest JK. Optimal design of trusses with geometric imperfections: accounting for global instability. Int J Solids Struct 2011;48:3011–9. https://doi.org/10.1016/J.IJSOLSTR.2011.06.020.

[25] Luo Y, Zhan J. Linear buckling topology optimization of reinforced thin-walled structures considering uncertain geometrical imperfections. Struct Multidiscip Optim 2020;62:3367–82. https://doi.org/10.1007/S00158-020-02738-6/TABLES/4.

[26] Movahedi Rad M, Habashneh M, Lógó J. Reliability based bi-directional evolutionary topology optimization of geometric and material nonlinear analysis with imperfections. Comput Struct 2023;287:107120. https://doi.org/10.1016/J.COMPSTRUC.2023.107120.

[27] Meng Z, Pang Y, Pu Y, Wang X. New hybrid reliability-based topology optimization method combining fuzzy and probabilistic models for handling epistemic and aleatory uncertainties. Comput Methods Appl Mech Eng 2020;363:112886. https://doi.org/10.1016/J.CMA.2020.112886.

[28] Madah H, Amir O. Concurrent structural optimization of buckling-resistant trusses and their initial imperfections. Int J Solids Struct 2019;162:244–58. https://doi.org/10.1016/J.IJSOLSTR.2018.12.007.

[29] Descamps B, Filomeno Coelho R. The nominal force method for truss geometry and topology optimization incorporating stability considerations. Int J Solids Struct 2014;51:2390–9. https://doi.org/10.1016/J.IJSOLSTR.2014.03.003.

[30] Fujii G, Akimoto Y, Takahashi M. Exploring optimal topology of thermal cloaks by CMA-ES. Appl Phys Lett 2018;112. https://doi.org/10.1063/1.5016090/35926.

[31] Meric RA. Material and load optimization of thermoelastic solids. Part I: sensitivity analysis. J Therm Stress 1986;9:359–72. https://doi.org/10.1080/01495738608961912.

[32] Li Q, Steven GP, Querin OM, Xie YM. Optimization of thin shell structures subjected to thermal loading. Struct Eng Mech Int J 1999;7:401–12. https://doi.org/10.12989/sem.1999.7.4.401.

[33] Rodrigues H, Fernandes P. A material based model for topology optimization of thermoelastic structures. Int J Numer Methods Eng 1995;38:1951–65. https://doi.org/10.1002/NME.1620381202.

[34] Li Q, Steven GP, Xie YM. Displacement minimization of thermoelastic structures by evolutionary thickness design. Comput Methods Appl Mech Eng 1999;179:361–78. https://doi.org/10.1016/S0045-7825(99)00047-X.

[35] Chung H, Amir O, Kim HA. Level-set topology optimization considering nonlinear thermoelasticity. Comput Methods Appl Mech Eng 2020;361:112735. https://doi.org/10.1016/J.CMA.2019.112735.

[36] Meng Z, Guo L, Yıldız AR, Wang X. Mixed reliability-oriented topology optimization for thermo-mechanical structures with multi-source uncertainties. Eng Comput 2022;38:5489–505. https://doi.org/10.1007/S00366-022-01662-1/FIGURES/17.
[37] Gao T, Xu P, Zhang W. Topology optimization of thermo-elastic structures with multiple materials under mass constraint. Comput Struct 2016;173:150–60. https://doi.org/10.1016/J.COMPSTRUC.2016.06.002.
[38] Habashneh M, Rad MM. Reliability based topology optimization of thermoelastic structures using bi-directional evolutionary structural optimization method. Int J Mech Mater Des 2023:1–16. https://doi.org/10.1007/S10999-023-09641-0/FIGURES/7.
[39] Yu Z, Ferrer-Argemi L, Lee J. Investigation of thermal conduction in symmetric and asymmetric nanoporous structures. J Appl Phys 2017;122. https://doi.org/10.1063/1.5006818/154704.
[40] Carstensen J., Ganobjak M. Topology-optimized design of building component with improved thermal and stiffness properties, 2018.
[41] Vantyghem G, De Corte W, Boel V, Steeman M. Structural and thermal performances of topological optimized masonry blocks. In: Proceedings of the Asian congress of structural and multidisciplinary optimization. 2016; 2016.
[42] Rad MM, Habashneh M, Cucuzza R, Domaneschi M, Melchiorre J. Enhancing thermal topology optimization with an elasto-plastic algorithm. In: Proceedings of the sixth international conference on soft computing, machine learning and optimisation in civil, structural and environmental engineering. 5; 2023. p. 1–7. https://doi.org/10.4203/CCC.5.1.6.
[43] McMeeking RM, Rice JR. Finite-element formulations for problems of large elastic-plastic deformation. Int J Solids Struct 1975;11:601–16. https://doi.org/10.1016/0020-7683(75)90033-5.
[44] Hsu TR. The finite element method in thermomechanics. The Finite Element Method in Thermomechanics. Springer; 1986. https://doi.org/10.1007/978-94-011-5998-2.
[45] Banas A, Hsu TR, Sun NS. Coupled thermoelastic-plastic stress analysis of solids by finite-element method. J Therm Stress 1987;10:319–44. https://doi.org/10.1080/01495738708927016.
[46] Xia L, Xia Q, Huang X, Xie YM. Bi-directional evolutionary structural optimization on advanced structures and materials: a comprehensive review. Arch Comput Methods Eng 2018;25:437–78. https://doi.org/10.1007/s11831-016-9203-2.
[47] Huang X, Xie YM. Convergent and mesh-independent solutions for the bi-directional evolutionary structural optimization method. Finite Elem Anal Des 2007;43:1039–49. https://doi.org/10.1016/j.finel.2007.06.006.
[48] Huang X, Xie M. Evolutionary topology optimization of continuum structures: methods and applications. John Wiley & Sons; 2010. https://doi.org/10.1002/9780470689486.
[49] Yang XY, Xie YM, Steven GP, Querin OM. Bidirectional evolutionary method for stiffness optimization. AIAA J 2012;37:1483–8. https://doi.org/10.2514/2.626.
[50] Huang X, Xie YM, Burry MC. Advantages of bi-directional evolutionary structural optimization (BESO) over evolutionary structural optimization (ESO). Adv Struct Eng 2007;10:727–37. https://doi.org/10.1260/136943307783571436.
[51] Dolamune Kankanamge N, Mahendran M. Behaviour and design of cold-formed steel beams subject to lateral–torsional buckling at elevated temperatures. Thin-Walled Struct 2012;61:213–28. https://doi.org/10.1016/J.TWS.2012.05.009.
[52] Prachar M, Hricak J, Jandera M, Wald F, Zhao B. Experiments of Class 4 open section beams at elevated temperature. Thin-Walled Struct 2016;98:2–18. https://doi.org/10.1016/J.TWS.2015.04.025.
[53] Schafer BW, Peköz T. Computational modeling of cold-formed steel: characterizing geometric imperfections and residual stresses. J Constr Steel Res 1998;47:193–210. https://doi.org/10.1016/S0143-974X(98)00007-8.
[54] Kankanamge ND, Mahendran M. Mechanical properties of cold-formed steels at elevated temperatures. Thin-Walled Struct 2011;49:26–44. https://doi.org/10.1016/J.TWS.2010.08.004.
[55] Ranawaka T, Mahendran M. Experimental study of the mechanical properties of light gauge cold-formed steels at elevated temperatures. Fire Saf J 2009;44:219–29. https://doi.org/10.1016/J.FIRESAF.2008.06.006.
[56] Lee JH, Mahendran M, Makelainen P. Prediction of mechanical properties of light gauge steels at elevated temperatures. J Constr Steel Res 2003;59:1517–32. https://doi.org/10.1016/S0143-974X(03)00087-7.
[57] European Committee for Standardization (CEN). Eurocode 3 design of steel structures-Part 1–2: general rules–structural fire design. Brussels: 2005.